Quantum Cluster Equilibrium Theory of Liquids: Temperature Dependence of Hydrogen Bonding in Liquid *N*-Methylacetamide Studied by IR Spectra

R. Ludwig,* O. Reis, and R. Winter

Physikalische Chemie, Fachbereich Chemie der Universität Dortmund, 44221 Dortmund, Germany

F. Weinhold and T. C. Farrar

Theoretical Chemistry Institute and Department of Chemistry, University of Wisconsin—Madison, Madison, Wisconsin 53706

Received: May 9, 1997; In Final Form: March 17, 1998

Temperature-dependent infrared spectra for liquid *N*-methylacetamide are calculated by the ab initio quantum cluster equilibrium (QCE) and Gaussian-94 methods and compared with experimental measurements. The calculations are based on standard ab initio self-consistent-field (SCF) methods at the 3-21G levels for five different molecular clusters. The cluster sizes vary from the monomer up to a five-membered linear structure. Strong cooperative effects are found in the molecular clusters and are reflected in the geometries and vibrational spectra for each species. The equilibrium populations of the clusters were calculated for the entire liquid range. At low temperatures the linear pentamer is the dominant species. At higher temperatures these clusters are replaced, primarily, by linear dimers and monomers. The calculated frequencies are in excellent agreement with the temperature behavior found in FT-IR experiments.

1. Introduction

Hydrogen-bonding interactions play an essential role in protein−ligand interactions and in the mechanism of peptide- and protein-mediated reactions.[1−3] The simplest protein model peptide system is *N*-methylacetamide ($NHCH_3COCH_3$ = NMA). Although NMA has been extensively studied by a variety of experimental[4−29] and theoretical[30−48] methods, uncertainties still exist concerning the effect of hydrogen bonding on its structure and conformation. Previous experimental NMA studies include Raman and infrared spectroscopy.[13−29] In addition, many theoretical normal-mode calculations have been carried out to obtain a best fit of the calculated frequencies with the experimental frequencies.[39−48] Spectra have been observed for gas-phase samples, for neat liquid samples, and for samples in aqueous solution; both hydrogen-bonded and non-hydrogen-bonded organic solvents were studied. None of these earlier studies include experimental infrared studies of liquid NMA which would allow a careful evaluation of the temperature dependence of hydrogen bonding.

Our experimental FT−IR measurements are focused on rigorous tests of a new theory for describing the equilibrium liquid properties of *N*-methylacetamide and other strongly H-bonded liquids: quantum cluster equilibrium (QCE) theory.[49] As the name implies, QCE theory is based on a full quantum treatment of the H-bonded clusters that are considered to be the constituent units of the liquid and gas (fluid) phases. The cluster equilibria that dictate phase composition are determined by the rigorous principles of quantum statistical thermodynamics in the canonical ensemble, based on the ab initio partition function for each cluster. From the equilibrium conditions, we obtain the QCE cluster population distribution that provides the proper weighting factors to compute the (*T*,*P*)-dependent equilibrium values of any desired cluster property such as infrared frequencies. Comparisons of QCE theoretical values with experimental measurements[50−54] provide stringent additional tests of the QCE-predicted population distributions and the associated (*T*,*P*)-dependent cluster picture of the equilibrium liquid structure.

The QCE population distributions tend to predict significantly different cluster patterns[49] than those found in molecular dynamics (MD) or Monte Carlo (MC) simulations using current empirical potentials.[55] We attribute these differences to systematic errors in the MD/MC potentials—specifically, omission (or underestimation) of the important quantal *cooperativity* effects associated with charge delocalization ("transfer") *between* monomers.[56] Such intermolecular charge transfer effects are physically distinct from monomer "polarization", and potentials based on the latter are inherently unsuitable for representing higher-order charge delocalization effects that become increasingly evident in stronger H bonds (such as those involving charged species, e.g., $F^- + HF$ or $OH^- + H_2O$). QCE is highly predictive, permitting experimental consequences of the novel liquid microstructures to be deduced by standard ab initio techniques for a broad range of structural, spectroscopic, and thermodynamic properties. The present work provides additional rigorous *T*-dependent experimental tests of this "surprising" QCE picture of the thermodynamic liquid phase. Additional details of the formalism and numerical convergence characteristics of the general QCE program[57] are presented elsewhere.[58,59]

In a recent article,[54] we used experimental NMR data to test the QCE model for describing the equilibrium liquid properties of *N*-methylacetamide. All available experimental NMR data were in reasonable qualitative or near-quantitative agreement with the theoretical QCE model. The present work describes complementary experimental FT-IR tests of the new theory. This provides additional information in three different areas: First, in contrast to the NMR parameters (quadrupole coupling

10.1021/jp971575u CCC: $15.00
Published on Web 10/21/1998

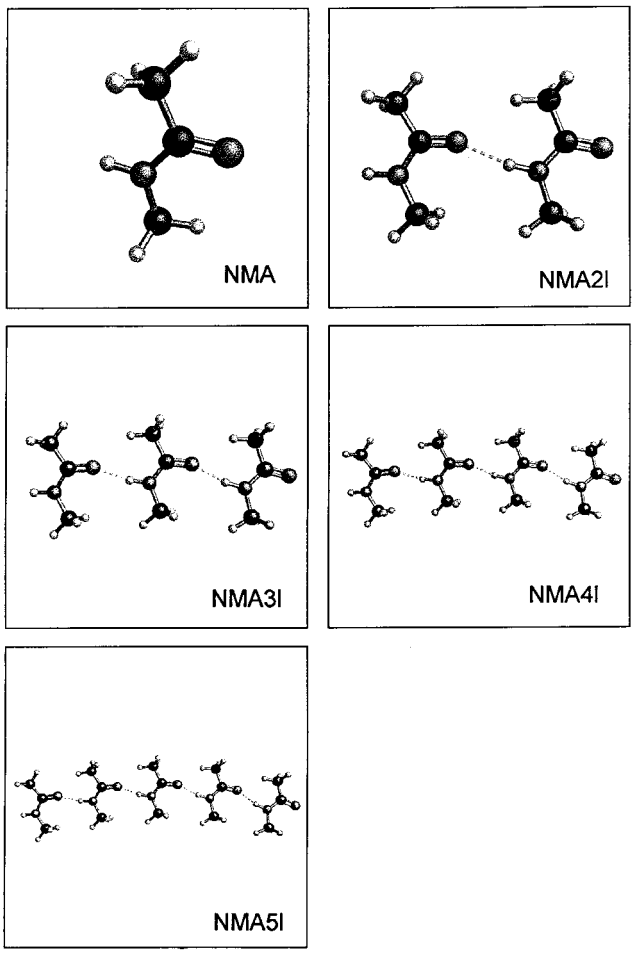

Figure 1. Equilibrium linear clusters of *trans-N*-methylacetamide.

constants and chemical shift values), calculated harmonic frequencies are used directly in the QCE model to calculate the cluster partition functions and to determine the cluster populations. A comparison with experimental data therefore allows a test of the accuracy of calculated harmonic frequencies and tests whether including vibrational anharmonicities and/or vibration rotation coupling is necessary for meaningful theoretical results. Second, on the NMR time scale, the solvation species are in fast exchange, and only time-averaged values may be measured. The time scale for vibrational spectroscopy is much faster, and therefore discrete solvates, including non-hydrogen-bonded, monosolvated, and multiply solvated species, can be observed. Third, calculated normal-mode vibrational frequencies play an important role in the assignment of experimental spectra and have a much more direct connection to the shape of the potential energy surface and thus to many other molecular properties that depend on this surface.

The computational methods used here are identical to those described in refs 54 and 58, including full geometry optimizations and harmonic frequencies. Ab initio calculations were carried out at the uncorrelated, restricted Hartree−Fock RHF/3-21G level for five NMA clusters $(NHCH_3COCH_3)_n$, $n = 1-5$. For completeness, the cluster structures and labels are shown in Figure 1.

2. Experimental Method

Infrared measurements were performed with a Nicolet Magna 550 FT-IR spectrometer equipped with a liquid nitrogen cooled mercury cadmium telluride (MCT) detector. An L.O.T.-Oriel variable-temperature cell equipped with CaF_2 windows and having a path length of 0.025 mm was used for the variable-temperature experiments.[60] Temperatures were maintained with an external Lauda RC 6 cryostat and were monitored with a NiCrNi (type K) thermocouple attached directly to the cell. The cell temperature was allowed to stabilize for at least 30 min before measurements were obtained; the cell temperature varied less than 0.5 °C during data acquisition. For each spectrum, 256 scans were coadded at a spectral resolution of 2 cm^{-1} and apodized with a Happ-Genzel function. Solvent subtraction was carried out by using reference spectra obtained at approximately the same temperatures as the sample spectra. The sample chamber was purged with dry, carbon dioxide-free air during data collection in order to minimize spectral contributions from atmospheric gases. *N*-Methylacetamide and CCl_4 were obtained from Aldrich Chemical Co., Inc., and used without further purification. One molar solutions of NMA in CCl_4 were used in all of the measurements.

TABLE 1: Ab Initio RHF/3-21G Geometries (in Å) Calculated for Different Molecular Clusters of NMA; Average Values Are Shown in Parentheses

geometry	NMA	NMA2l	NMA3l	NMA4l	NMA5l
r_{NH}	0.9949	0.9948	0.9957	0.9958	0.9958
		1.0009	1.0032	1.0040	1.0043
			1.0031	1.0062	1.0071
				1.0039	1.0072
					1.0043
	(0.9949)	(0.9979)	(1.0007)	(1.0027)	(1.0037)
r_{CO}	1.2199	1.2278	1.2271	1.2276	1.2279
		1.2235	1.2325	1.2345	1.2352
			1.2246	1.2342	1.2363
				1.2251	1.2347
					1.2253
	(1.2199)	(1.2257)	(1.2281)	(1.2304)	(1.2319)
r_{CN}	1.3542	1.3421	1.3438	1.3332	1.3430
		1.3467	1.3354	1.3333	1.3326
			1.3456	1.3337	1.3315
				1.3451	1.3332
					1.3448
	(1.3542)	(1.3444)	(1.3416)	(1.3388)	(1.3370)
r_{N-O}		2.9096	2.8753	2.8638	2.8595
			2.8719	2.8254	2.8129
				2.8608	2.8136
					2.8570
		(2.9096)	(2.8736)	(2.8500)	(2.8358)

3. Results and Discussion

3.1. Cluster, Structural, Energetic, and Infrared Properties. As shown in Figure 1 (and used in all the tables), we employ the labels NMA, NMA2l, NMA3l, NMA4l, and NMA5l for linear dimer, trimer, tetramer, and pentamer, respectively.[61] Because of computational limitations, clusters larger than pentamers were not possible.[62]

The strong effects of *cooperative* (nonpairwise-additive) contributions to H-bonding energetics were previously noted.[54] These arise from intermolecular electron delocalization ("charge transfer") aspects of H-bonding which are enhanced in the bicoordinate patterns of Figure 1.[63] This cooperative enhancement was also found to give interesting geometries for the different NMA clusters, as summarized in Table 1. For example, as a consequence of cooperative enhancement, r_{NC} decreases by about 1.7 pm and r_{CO} increases by about 1.2 pm going from the monomer up to the five-membered linear cluster values. A similar observation has been made by Otterson[31] comparing C−O and C−N bond lengths in solid and gaseous formamide and by Zeidler[64] comparing gas-phase geometries with the liquid structure of *N*-methylformamide. Cooperative

TABLE 2: Ab Initio Harmonic Frequencies $\bar{\nu}$ in cm^{-1} for N−H, C═O, and C−N(O) Stretches in Different Clusters of NMA Obtained with 3-21G Basis

	N−H			C═O			N−C(O)		
cluster	$\bar{\nu}$/cm^{-1}	scaled	*A*	$\bar{\nu}$/cm^{-1}	scaled	*A*	$\bar{\nu}$/cm^{-1}	scaled	*A*
NMA	3833.2	3411.6	36.26	1897.2	1688.5	233.5	1708.3	1520.4	98.6
av	3833.2	3411.6	36.26	1897.2	1688.5	233.5	1708.3	1520.4	98.6
NMA2l	3758.0	3411.6	36.26	1869.3	1663.7	590.1	1701.1	1514.0	127.3
	3841.3	3318.8	53.4	1886.6	44.6	1679.1	1741.8	1550.2	232.5
av	3765.4	3351.2		1870.5	1664.8		1727.4	1537.4	
NMA3l	3710.3	3302.1	1391.1	1852.2	1648.5	1701.5	1514.4	160.6	
	3721.8	3312.4	27.7	1870.9	1665.1	62.9	1751.3	1558.7	74.1
	3839.4	3417.0	58.3	1884.3	1677.0	117.5	1753.1	1560.3	532.7
av	3715.8	3307.1		1857.1	1652.9		1742.0	1550.3	
NMA4l	3660.6	3257.9	1479.1	1844.6	1641.7	1131.0	1701.7	1514.6	173.8
	3701.6	3294.5	475.1	1860.4	1655.7	24.6	1754.5	1561.5	279.7
	3705.6	3298.0	514.4	1869.6	1664.0	144.2	1755.4	1562.3	424.5
	3838.6	3416.3	60.1	1883.7	1676.5	107.6	1762.0	1568.2	384.2
av	3681.7	3276.7		1850.8	1647.2		1748.9	1556.6	
NMA5l	3636.6	3236.6	2458.2	1840.8	1638.3	1345.9	1701.8	1514.6	179.2
	3652.5	3250.7	30.7	1853.2	1649.3	50.7	1755.5	1562.4	372.1
	3696.0	3289.4	565.1	1863.2	1658.2	131.5	1756.1	1562.9	485.9
	3700.6	3293.5	547.3	1868.9	1663.3	87.3	1763.5	1569.5	749.1
	3838.2	3416.0	61.0	1883.3	1676.2	109.4	1765.3	1571.1	27.6
av	3658.9	3256.4		1846.8	1643.7		1753.6	1560.7	

[a] For comparison with the experimental vibration spectra as well as for the use in the QCE model all frequencies are scaled by a factor of 0.89. The average values for each cluster are obtained by weighting the frequencies with the appropriate calculated absorbance *A*.

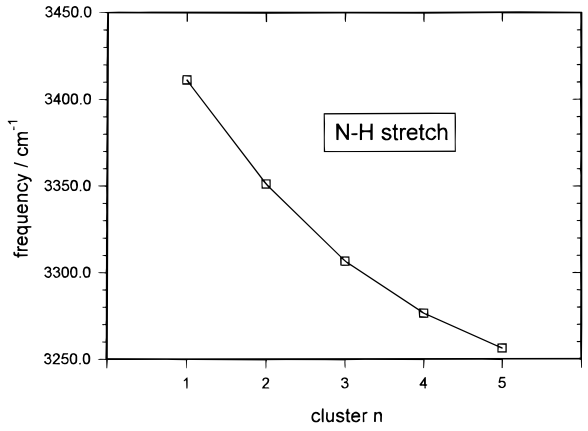

Figure 2. Calculated average N−H stretch frequencies in *N*-methylacetamide as a function of cluster size.

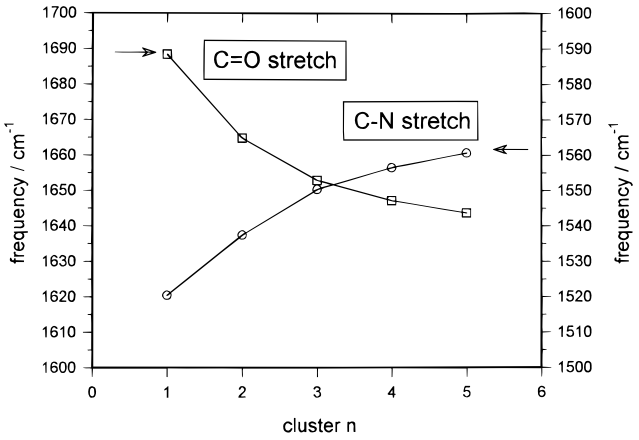

Figure 3. Calculated average C═O and C−N stretch values in *N*-methylacetamide as a function of cluster size.

geometry changes are also evident in the N−H···O bonding region, where the covalent N−H bond lengthens by about 0.9 pm while the intermolecular N···O distance decreases from 291 pm (dimer) to 284 pm (pentamer).

The calculated frequencies show a similar behavior. In the simulated spectra the RHF/3-21G theoretical frequencies were all multiplied by the standard scale factor, 0.89, to correct for known systematic errors of the Hartree−Fock approximation.[65] It may be noted that such uniform scaling does not alter the ab initio predicted normal modes and intensities. These uniformly scaled frequencies are used in the discussion below. All frequencies for the N−H, C═O, and C−N stretches as well as their intensities are listed in Table 2. In the trimer, NMA3l, for example, there exist three different N−H stretch frequencies that depend on the position of the molecule within the cluster. Two lower frequencies of about 3302 and 3312 cm^{-1} are predicted for N−H bonds that are involved in hydrogen bonding, and one higher frequency of about 3417 cm^{-1} is calculated for the free, terminal N−H bond.

The average frequency calculated for the N−H stretch in a linear trimer is about 3307 cm^{-1}. The average values are obtained by weighting the different single frequencies with their calculated intensities, *A*. These values are also given in Table 2. The average N−H stretch frequencies for the monomer up through the pentamer are shown as a function of cluster size in Figure 2, leading to variations of 150−200 cm^{-1}. This large shift is caused by strong cooperative effects and should be readily detectable in an IR experiment (as discussed below). Similar theoretical results are obtained for the C═O stretch. An increasing cluster size leads to longer average C═O bond lengths, decreasing force constants and therefore smaller wavenumbers, as shown in Figure 3. The opposite behavior is found for the C−N stretch; this is also shown in Figure 3. Here, with increasing cluster size the C−N bond is shortened, and the frequencies move to higher wavenumbers. Unfortunately, the C═O and the C−N stretch frequencies shift by only about 40 cm^{-1} between the monomer and the linear pentamer, making their detection more difficult in an IR experiment.

3.2. Experimental IR Frequencies. Since the absorbance for pure *N*-methylacetamide was too large to carry out experiments in the neat liquid, we recorded the FT-IR spectra of solutions of NMA. Carbon tetrachloride was chosen as the solvent since it interacts only very weakly with NMA and similar compounds.[66,67] In contrast to hydrogen-bonding solvents such as dioxane and water, CCl_4 does not disrupt intermolecular amide−amide hydrogen bonding.[68−70] For neat

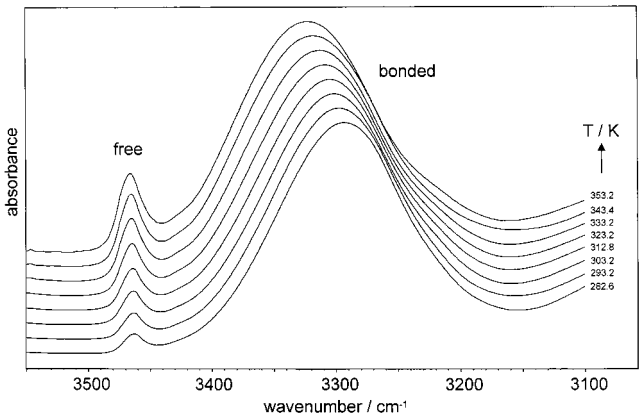

Figure 4. N−H stretch region FT-IR spectral data for 1 M *N*-methylacetamide solution in CCl_4 as a function of temperature. The sharp bands at 3450−3480 cm^{-1} are assigned to non-hydrogen-bonded N−H, and the broad bands at 3200−3400 cm^{-1} are assigned to hydrogen-bonded N−H.

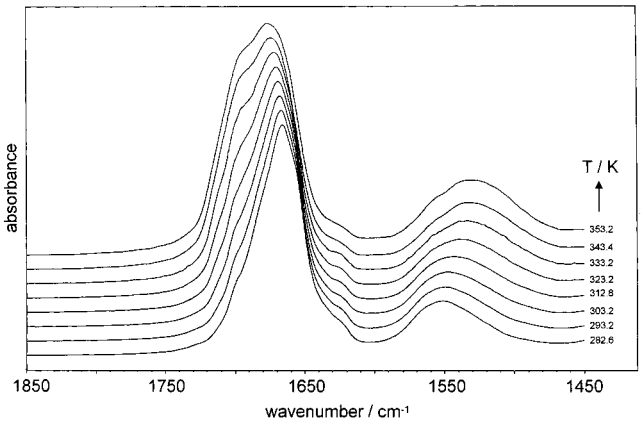

Figure 5. C═O and C−N stretch region FT-IR spectral data for 1 M *N*-methylacetamide solution in CCl_4 as a function of temperature. The broad bands at 1665−1675 cm^{-1} are assigned to hydrogen-bonded C═O.

NMA, a low-resolution IR spectrum is available in the Merck FT-IR atlas. Here one observes IR stretch frequencies for both hydrogen-bonded and terminal NH groups in neat, liquid NMA.[71]

The measurements reported here are for a 1.0 M solution of NMA in CCl_4. Recent dielectric relaxation experiments of *N*-methylacetamide in CCl_4 solutions have been carried out for concentrations between 0.0016 and 1.5 mol dm^{-3}.[10] Above an NMA concentration of about 0.8 mol dm^{-3} the relaxation time associated with changes in hydrogen bonding no longer increases, but instead reaches a constant value. Similarly, concentration-dependent studies of the isotopic chemical shifts of NMA−CCl_4 binary mixtures show that the chemical shifts all reach their asymptotic limits at a concentration of about 1.0 M.[72] That is, at concentrations higher than 0.8 mol dm^{-3} the cluster populations of NMA are comparable to those in higher concentrations and in the neat liquid. For the neat liquid, QCE calculations predict that the most significant populations are linear pentamer (40%), linear dimer (20%), and monomer (17%).

The experimental IR spectra for temperatures between 283 and 353 K are shown in Figures 4 and 5. For comparison with our theoretical results, we focus on the N−H, C═O, and C−N stretching motions. The temperature dependence of these parameters is shown in Table 3. In the literature it is common practice to label the vibrations originating predominantly from the amide groups in decreasing order of vibrational frequency as amide A, I, II, etc. Amide A refers to the N−H stretch frequencies (Figure 4), amide I refers to the C═O stretch, and amide II refers to the (O)C−N stretching with significant mixing from in-plane N−H bending (Figure 5). The amide A, I, and II absorption bands, predicted to be at about 3250−3300, 1630−1700, and 1510−1570 cm^{-1}, respectively, have large intensities for all of the *trans*-NMA conformers.

TABLE 3: Calculated Harmonic Frequencies (cm^{-1}) in Liquid NMA

T (K)	N−H str	C═O str	C−N(O) str
303	3339.6	1653.2	1555.5
313	3344.5	1654.9	1554.0
323	3349.1	1656.6	1552.5
333	3355.0	1658.6	1550.9
343	3358.2	1659.7	1550.0
353	3362.4	1661.1	1548.8
363	3366.0	1662.4	1547.8
373	3368.9	1663.5	1546.8
383	3371.8	1664.6	1545.9
393	3374.8	1665.6	1545.1
403	3376.5	1666.4	1544.3
413	3378.9	1667.3	1543.6
423	3380.8	1668.0	1543.0
433	3382.5	1668.7	1542.4
443	3383.6	1669.3	1541.8
453	3385.6	1669.9	1541.4
463	3386.3	1670.4	1541.0
473	3387.5	1670.8	1540.6
478	3387.7	1671.0	1540.4

The experimental amide *A* stretch frequencies are shown in Figure 4. The absorption bands for the free and the hydrogen-bonded N−H bonds are separated nicely at all temperatures. The ability to see the individual frequencies for both the hydrogen-bonded and the terminal NH bonds provides much more detailed information than the NMR data, which gives only average values for isotropic chemical shifts and quadrupole coupling constants. This is due to the fact that equilibration between hydrogen-bonded and non-hydrogen-bonded states for a given amide proton is fast on the NMR time scale; consequently, the observed amide chemical shift and quadrupole coupling constant values are weighted averages of the values in the different environments.

In contrast to the hydrogen-bonded NH stretch frequency which moves by about 30 cm^{-1} (to lower wavenumbers) over the observed temperature range, the free N−H frequency is essentially temperature independent. The intensity of the free N−H frequency, relative to the bonded NH frequency, increases with increasing temperature. The experimental amide I and II stretch frequencies are shown in Figure 5. Increasing temperature leads to different behaviors for the C═O and C−N stretching motion. Over the temperature range studied, the C═O frequency moves by about 10 cm^{-1} to longer wavenumbers and the C−N stretch frequency decreases by 15 cm^{-1}. These observations agree well with the theoretical prediction.

3.3. QCE Population Distributions and Temperature-Dependent Frequencies. For comparison with the observed infrared spectra, we weighted the calculated average N−H, C═O, and C−N stretching frequencies with the appropriate cluster population (as reported in ref 54) at each temperature; at 303 K the cluster populations for the five linear species ranging from monomer up to linear pentamer are 16.5, 20.3, 10.2, 12.7, and 40.4%, respectively. The temperature-dependent frequencies obtained for all modes are listed in Table 3. Because the calculated intensities for the resonances are not very reliable, we focus our comparison on the temperature-dependent shift of the maximum values for each stretching mode.

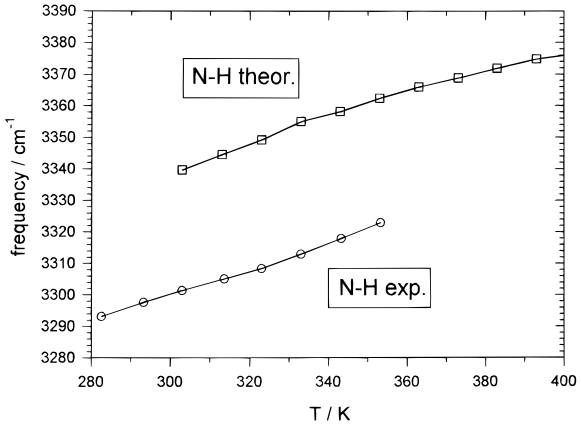

Figure 6. Calculated (open squares) and experimental (open circles) N−H stretch values in liquid *N*-methylacetamide as a function of temperature. See text for details of the calculated values.

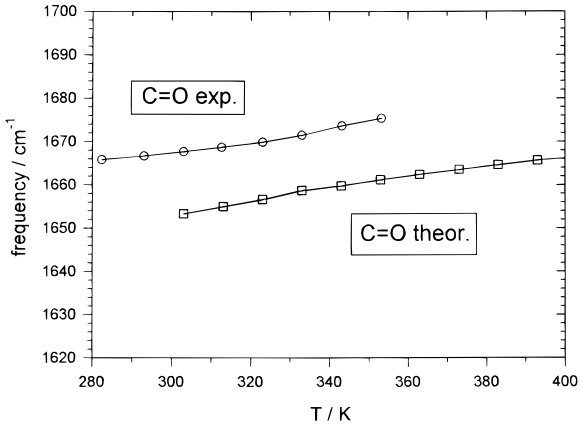

Figure 7. Calculated (open squares) and experimental (open circles) C═O stretch values in liquid *N*-methylacetamide as a function of temperature.

For the N−H stretch, good agreement is obtained between the experimental and the calculated values, as summarized in Figure 6. Both N−H stretch frequencies move to larger wavenumbers with increasing temperature because of hydrogen bond breaking. The slope of the temperature dependence is nearly the same for both modes, and both are in rather nice agreement with theory.

The temperature dependence of the N−H stretch can be used like the amide proton NMR chemical shifts ($\delta\sigma/\delta$T) as a tool for studying inter- and intramolecular hydrogen-bonding peptides.[17,73,74] Small $\delta\sigma/\delta$T values are usually interpreted as evidence for a hydrogen-bonded N−H; larger $\delta\sigma/\delta$T values suggest a solvent-exposed, non-hydrogen-bonded N−H. Our experimental NMR studies[54] show that large $\delta\sigma/\delta$T values are obtained even for pure hydrogen-bonding liquids. Our NMR calculations indicate that this result is caused by cooperative electronic changes of the NMA molecules within the clusters. The temperature behavior of the N−H stretch is well correlated with the r_{NH} bond length. Even the small changes of about 0.2 pm over this temperature range cause a significant shift of more than 26 cm^{-1}. As with chemical shifts, the IR frequencies are very sensitive to small changes in the electronic environment. Unfortunately, the predicted geometric changes are too small to be directly detected with neutron or X-ray diffraction methods, but both IR and NMR measurements provide strong indirect evidence for these changes.

In Figure 7 the calculated C═O frequencies are compared with the experimental data. Both frequencies move to higher wavenumbers with increasing temperature. The slope in both cases is almost identical. Over the temperature range observed (303−353 K), the theoretical data shift by about 8 cm^{-1}, in good agreement with the shift of 7 cm^{-1} found experimentally. The very different temperature dependence of the N−H versus the C═O stretch found in the experiment is nearly quantitatively reflected in the calculated properties by the QCE model. The temperature dependence of both stretching modes is attributed to decreasing bond lengths r_{NH} and r_{CO}. This agrees with the result of Cheam and Krimm,[41] who found that the decrease in the N−H stretch and C═O stretch harmonic force constants on hydrogen bonding are due primarily to increases in the length of the NH and CO bonds.

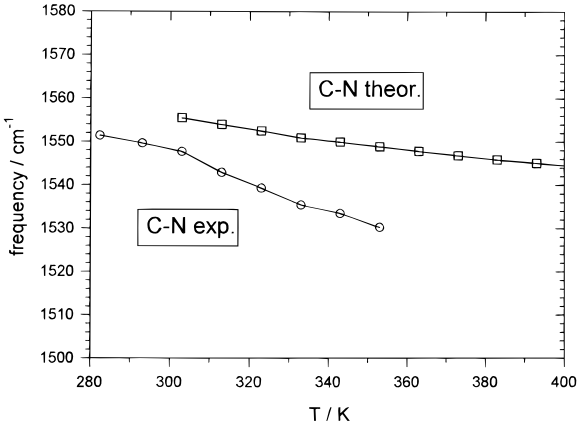

Figure 8. Calculated (open squares) and experimental (open circles) C−N stretch values in liquid *N*-methylacetamide as a function of temperature.

The opposite temperature-dependent behavior is found for the C−N stretching motion, as shown in Figure 8. Both theory and experiment show that the frequencies shift to smaller wavenumbers with increasing temperature. The behavior for the C−N and C═O stretch frequencies is again related to the temperature-dependent behavior of the molecular geometry (see Table 1). Decreasing C═O bond lengths lead to increasing force constants and vibrational frequencies whereas increasing C−N bond lengths lead to smaller bond lengths and stretching frequencies. In contrast to the N−H and C═O stretching motions, the calculated C−N frequencies are in good agreement with the experimental infrared spectrum only at lower temperatures. At higher temperatures the experimental C−N stretch drops more rapidly to lower wavenumbers than predicted by theory. This is most likely due to the fact that the experimental infrared spectrum includes contributions from C−N−H in-plane bending motions, so that small changes in the composition of the normal mode have a relatively large effect on frequency. The C−N−H in-plane bending motion is mainly determined by the bond angle C−N−H. As can be seen in Figure 1, the calculated bond angle may be strongly influenced by the position of the methyl groups. This complication is probably the source of the differences between theory and experiment for the C−N stretching motion at higher temperatures. Different orientations of the methyl groups may also change the N−C−O bond angle and could therefore have some influence on the C═O stretching motion. But, as shown above, this frequency is primarily determined by the C═O bond length, and good agreement between the calculated and experimental values is found.

The opposing shift of the CN stretching frequency, relative to NH and CO frequencies, can be readily rationalized in terms of the "charge transfer" or "resonance" picture of H bonding.[49] Since the H-bond is pictured as having significant "resonance

hybrid" character ($A-H:B \rightleftarrows A:^{-}H-B^{+}$, it necessarily *couples* to other types of resonance delocalization, such as the well-known amide resonance of NMA ($N-C{=}O \rightleftarrows N^{+}{=}C-O-$). Just as H bonding is known to be enhanced by resonance,[75] so does formation of H bonds *strengthen* the resonance in the participating amide groups, increasing the CN double-bond character (and blue-shifting its stretching frequency) while decreasing the CO bond order (and red-shifting its frequency). The pattern of temperature-dependent frequency shifts is therefore fully consistent with this simple picture of coupled intramolecular/intermolecular resonance delocalization.

4. Conclusions

The temperature-dependent experimental infrared results reported here provide a further quantitative experimental test of the ab initio QCE/3-21G model of liquids. As with the temperature-dependent chemical shift and quadrupole coupling experiments, the experimental infrared date are in good overall agreement with the theoretical predictions of the QCE model. Additional experimental work could provide even more stringent tests of the theory. For example, temperature-dependent infrared studies with isotopically substituted compounds would allow one to distinguish the different kinds of IR modes that are present. Pressure-dependent NMR and IR experiments are also desirable in order to test the ability of the QCE model to predict pressure-dependent behavior.

Further improvements in the QCE theory are in progress. These improvements include the use of higher basis set levels and the inclusion of correlation effects. The present QCE treatment employs two empirical parameters (the mean field coefficient and excluded-volume correction factor) that have little influence on qualitative clustering patterns and are be used to fix the density and boiling point at a single pressure. For infrared studies the inclusion of vibrational anharmonicities and vibration−rotation coupling is desirable.

The present experimental results along with previous NMR results (chemical shifts and quadrupole coupling constants) for water, formamide, and *N*-methylformamide[50−54] suggest that the QCE methodology can be applied successfully to a variety of liquid types with markedly different clustering patterns. Current studies in this laboratory are devoted to a much broader spectrum of H-bonded liquids, including binary solutions, that will further test the limits of the QCE approach.

Acknowledgment. We thank the National Science Foundation, Grant CHE-9500735, for the support of this research. R.L. thanks the Deutsche Forschungsgemeinschaft and the Fonds der Chemischen Industrie for financial support. We thank Mark Wendt for help with some of the drawings.

References and Notes

(1) Kuntz, I. D., Jr., Kauzmann, W. *Adv. Protein Chem.* **1974**, *28*, 239.
(2) Packer, L. *Methods Enzymol.* **1986**, *127*, 1−416.
(3) Sundaralingam, M.; Sekharudu, Y. C. *Science* **1989**, *244*, 1333.
(4) Kitano, M.; Fukuyama, T.; Kuchitsu, K. *Bull. Chem. Soc. Jpn.* **1973**, *46*, 384.
(5) Katz, J. L.; Post, P. *Acta Crystallogr.* **1960**, *13*, 624.
(6) Itoh, K.; Shimanouchi, T. *Bioploymers* **1967**, *5*, 921.
(7) Hamazaoui, F.; Baert, F. *Acta Crystallogr.* **1994**, *C50*, 757.
(8) Burgar, M.; St. Amour, T. E.; Fiat, D. *J. Chem. Phys.* **1981**, *85*, 502.
(9) Glushka, J.; Lee, M.; Coffin, S.; Cowburn, D. *J. Am. Chem. Soc.* **1989**, *111*, 7716.
(10) Omar, M. M. *J. Chem. Soc., Faraday Trans. 1* **1978**, *74*, 115.
(11) Pralat, K.; Jadzyn, J.; Balanicka, S. *J. Chem. Phys.* **1983**, *87*, 1385.
(12) Häseler, S.; Poglitisch, A.; Bechthold, G.; Genzel, L. *J. Chem. Phys.* **1987**, *86*, 4327.
(13) Fillaux, F.; Baron, M. H. *Chem. Phys.* **1981**, *62*, 275.
(14) Fillaux, F.; De Loze, C. *Chem. Phys. Lett.* **1976**, *36*, 547.
(15) Polavarapu, P. L.; Deng, Z.; Ewig, C. S. *J. Phys. Chem.* **1994**, *98*, 9819.
(16) Kuznetsova, L. M.; Furer, V. L.; Maklakov, L. I. *J. Mol. Struct.* **1996**, *380*, 23.
(17) Gellman, S. H.; Dado, G. P.; Liang, G.-B.; Adams, B. R. *J. Am. Chem. Soc.* **1991**, *113*, 1164.
(18) Mayne, L. C.; Ziegler, L. D.; Hudson, B. *J. Chem. Phys.* **1985**, *89*, 3395.
(19) Nielson, O. F.; Christensen, D. H.; Rasmussen, O. H. *J. Mol. Struct.* **1991**, *242*, 273.
(20) Wang, Y.; Purcello, R.; Georghiou, S.; Spiro, T. G. *J. Am. Chem. Soc.* **1991**, *113*, 6368. 6359.
(21) Triggs, N. E.; Valetini, J. J. *J. Phys. Chem.* **1992**, *96*, 6922.
(22) Didik, J. M.; Johnson, C. R.; Asher, S. A. *J. Phys. Chem.* **1985**, *89*, 3805.
(23) Harada, I.; Sugawara, Y.; Matsuara, H.; Shimanouchi, T. *J. Raman Spectrosc.* **1975**, *4*, 91.
(24) Song, S.; Asher, S. A.; Krimm, S.; Bandekar, J. *J. Am. Chem. Soc.* **1988**, *110*, 8547.
(25) Song, S.; Asher, S. A.; Shaw, K. D. *J. Am. Chem. Soc.* **1991**, *113*, 1155.
(26) Chen, X. G.; Asher, S. A.; Schweitzer-Stenner, R.; Mirkin, N. G.; Krimm, S. J. *J. Am. Chem. Soc.* **1995**, *117*, 2884.
(27) Mayne, L. C.; Hudson, B. S. *J. Phys. Chem.* **1991**, *95*, 2962.
(28) Gerothanassis, I.; Vakka, C. *J. Org. Chem.* **1994**, *59*, 2341.
(29) Akiyama, M.; Othani, T. Spectrochim. Acta, **1994**, 50, 317.
(30) Mirkin, N. G.; Krimm, S. *J. Mol. Struct.* **1991**, *242*, 143.
(31) Otterson, T. *Adv. Mol. Relax. Prodesses* **1976**, *9*, 105.
(32) Yu, H. A.; Karplus, M.; Petitt, B. M. *J. Am. Chem. Soc.* **1991**, *113*, 2435.
(33) Guo, H.; Karplus, M. *J. Phys. Chem.* **1992**, *96*, 7273.
(34) Guo, H.; Karplus, M. *J. Phys. Chem.* **1994**, *98*, 7104.
(35) Luque, F. J.; Orozco, M. *J. Org. Chem.* **1993**, *58*, 6397.
(36) Radom, L.; Riggs, N. V. *Aust. J. Chem.* **1982**, *35*, 1071.
(37) Jorgensen, W. L.; Gao, J. L. *J. Am. Chem. Soc.* **1988**, *110*, 4212.
(38) Cieplak, P.; Kollmann, P. *J. Comput. Chem.* **1991**, *12*, 1232.
(39) Sugawara, Y.; Hirakawa, A. Y.; Tsuboi, M. *J. Mol. Struct.* **1984**, *108*, 206.
(40) Sugawara, Y.; Hirakawa, A. Y.; Tsubori, M.; Kato, S.; Morokuma, M. *J. Mol. Spectrosc.* **1986**, *115*, 21.
(41) Cheam, T. C.; Krimm, S. *J. Mol. Struct.* **1986**, *146*, 175.
(42) Forgarasi, G.; Pulay, P.; Torok, F. *J. Mol. Struct.* **1979**, *57*, 259.
(43) Balazs, A. *J. Mol. Struct.* **1979**, *57*, 259.
(44) Williams, R. W. *Biopolymers* **1992**, *32*, 829.
(45) Cheam, T. C. *J. Mol. Struct.* **1992**, *257*, 57.
(46) Mirkin, N. G.; Krimm, S. *J. Am. Chem. Soc.* **1991**, *113*, 9742.
(47) Ataka, S.; Takeuchi, H.; Tasumi, M. *J. Mol. Struct.* **1984**, *113*, 147.
(48) Radzicka, A.; Pedersen, L.; Wolfenden, R. *Biochemistry* **1988**, *27*, 4538.
(49) Weinhold, F. *J. Mol. Struct.* (*THEOCHEM*) **1997**, *399*, 181.
(50) Ludwig, R.; Weinhold, F.; Farrar, T. C. *J. Chem. Phys.* **1995**, *103*, 6941.
(51) Ludwig, R.; Weinhold, F.; Farrar, T. C. *J. Chem. Phys.* **1995**, *102*, 5118.
(52) Ludwig, R.; Weinhold, F.; Farrar, T. C. *J. Chem. Phys.* **1995**, *103*, 3636.
(53) Ludwig, R.; Weinhold, F.; Farrar, T. C. *J. Phys. Chem.* **1997**, *107*, 499.
(54) Ludwig, R.; Weinhold, F.; Farrar, T. C. *J. Chem. Phys.* in press.
(55) Leach, A. R. *Molecular Modelling, Principles and Applications*. Addison-Wesley Longman: Essex, England, 1996; Chapter 6.
(56) Reed, A. E.; Curtiss, L. A.; Weinhold, F. *Chem. Rev.* **1988**, *88*, 899.
(57) *QCE 1.0*: Weinhold, F. Theoretical Chemistry Institute, University of Wisconsin, Madison, 1998.
(58) Weinhold, F.; Quantum Cluster Equilibrium Theory of Liquids: General Theory and Computer Implementation, University of Wisconsin Theoretical Chemistry Institute Technical Report WIS-TCI-883, 1998; submitted for publication.
(59) Weinhold, F. Quantum Cluster Equilibrium Theory of Liquids: Illustrative Application to H_2O, University of Wisconsin Theoretical Chemistry Institute Technical Report WIS-TCI-884, 1998; submitted for publication.
(60) The 25 μm cell path permitted measurements up to the maximum 1.0 M CCl_4 solution concentration reported here. A planned 12 μm cell configuration should permit additional measurements to test the asymptotic dependence at higher concentrations.
(61) Note that other possible cluster types (such as the antiparallel arrangements of the crystalline phase) were examined but ultimately excluded from further consideration because (1) they achieved no significant QCE population at any part of the liquid range or (2) they were not true stationary points on the RHF/3-21G surface.

(62) Although the hexamer was optimized, its frequencies could not be obtained within available disk resources. Note however that structural and energetic differences diminish significantly at higher *n* (as cooperativity effects "saturate" with longer chain lengths), so that omission of such higher homologues (even if their populations were significant) is unlikely to strongly affect calculated QCE properties. Linear clusters larger than pentamers were found to be highly unlikely for formamide (ref 51).

(63) Note (as described in ref 54) that all binding energies were corrected by the standard counterpoise procedure to suppress effects of basis set superposition error. Cooperative enhancement patterns are generally found to be much less affected by counterpoise corrections than is the pairwise (dimer) energy.

(64) Neuefeind, J.; Chieux, P.; Zeidler, M. D. *Mol. Phys.* **1992**, *676*, 143.

(65) Hehre, W. J.; Radom, L.; Schleyer, P. v. R.; Pople, J. A. *Ab Initio Molecular Orbital Theory*; Wiley: New York, 1986; p 229.

(66) Becker, E. D.; Liddel, U.; Shoolery, J. N. *J. Mol. Spectrosc.* **1958**, *2*, 1.

(67) Wendt, M.; Meiler, J.; Weinhold, F.; Farrar, T. C. *Mol. Phys.* **1998**, *93*, 145.

(68) Klotz, I. M.; Franzen, J. S. *J. Am. Chem. Soc.* **1962**, *84*, 3461.

(69) Krikorian, S. E. *J. Chem. Phys.* **1982**, *86*, 1875.

(70) Graham, L. L.; Chang, C. Y. *J. Chem. Phys.* **1971**, *75*, 784.

(71) Merck, *FT-IR Atlas*; edited by Merck, Darmstadt in Collaboration with Bruker Analytische Messtechnik GmbH, Karlsruhe, VCH Verlag: Weinheim, 1988.

(72) Graham, L. L.; Chang, C. Y. *J. Chem. Phys.* **1971**, *75*, 776.

(73) Rose, G. D.; Gierasch, L.; Smith, J. *Adv. Protein Chem.* **1985**, *37*, 1.

(74) Kessler, H. *Angew. Chem., Int. Ed. Engl.* **1982**, *21*, 512.

(75) Gilli, P.; Ferretti, V.; Bertolasi, V.; Filli, G. *Adv. Mol. Struct. Res.* **1996**, *2*, 67.